Pollen-based seasonal temperature reconstruction in Northeast China over the past 10,000 years, and its implications for understanding the Holocene Temperature Conundrum

Rongwei Geng [a,b], Yan Zhao [b,c,*], Ulrike Herzschuh [d,e,f], Qiaoyu Cui [b], Zhuo Zheng [g], Xiayun Xiao [h], Chunmei Ma [i], Chen Liang [j]

[a] Cluster of Excellence ROOTS, Kiel University, 24118 Kiel, Germany
[b] Key Laboratory of Land Surface Pattern and Simulation, Institute of Geographic Sciences and Natural Resources Research, Chinese Academy of Sciences, 100101 Beijing, China
[c] College of Earth and Planetary Sciences, University of Chinese Academy of Sciences, 100049 Beijing, China
[d] Polar Terrestrial Environmental Systems, Alfred Wegener Institute Helmholtz Center for Polar and Marine Research, 14473 Potsdam, Germany
[e] Institute of Environmental Science and Geography, University of Potsdam, 14476, Germany
[f] Institute of Biochemistry and Biology, University of Potsdam, 14476, Germany
[g] School of Earth Sciences and Engineering, Sun Yat-Sen University, 51900 Zhuhai, China
[h] Nanjing Institute of Geography and Limnology, Chinese Academy of Sciences, 210008 Nanjing, China
[i] School of Geography and Ocean Science, Nanjing University, 210023 Nanjing, China.
[j] School of Land Science and Space Planning, Hebei GEO University, 050031 Shijiazhuang, China

ARTICLE INFO

ABSTRACT

The Holocene Temperature Conundrum refers to the mismatch between proxy-based temperature records and those based on climate model simulations. A possible reason for this mismatch is a putative proxy-based bias in reconstructed summer temperatures, and therefore, regional reconstructions of seasonal temperature are crucial for resolving the conundrum. In this paper, we reconstruct vegetation and climate changes over the last ~10,000 years BP based on a high-resolution pollen record from Gushantun peatland, Changbai Mountains, Northeast China. Multiple quantitative reconstruction approaches were used and weighted averaging partial least squares regression (WAPLS) was found to be the most appropriate method for reconstructing Holocene temperature and precipitation. The reconstructed climate record shows that the Holocene Climate Optimum occurred between 8 ka and 6 ka and exhibited a cold month mean temperature that was 3 °C warmer than modern temperatures. Climate gradually cooled during late Holocene with a minimum cold month temperature of −19.6 °C. Four prominent cold events occurred around 8.7 ka BP, 7.8 ka BP, 5.7 ka BP, and 2.5 ka BP with an amplitude variation up to 3 °C. The synthesized seasonal temperature time series and a comparison with other proxies show that the decreasing trend in mean annual temperature is not a seasonal bias caused by summer temperature change. This study provides evidence of a Holocene seasonal temperature change at a regional scale and insights for further understanding of the Holocene Temperature Conundrum.

1. Introduction

The Holocene Temperature Conundrum has been the subject of intense debate in the studies of Holocene climate change. It is the discrepancy of diverging annual temperature change between the cooling trend from the proxy-based reconstructions and the warming trend from climate model simulations (Jiang et al., 2012; Kaufman et al., 2020; Kaufman and Broadman, 2023; Liu et al., 2014; Marcott et al., 2013). The current main driving mechanisms (e.g. greenhouse gases and ice sheets) based on simulation yield warming trends, and the possible bias can be caused by differences in the sensitivity of climate models to the forcings and other feedback mechanisms (Bader et al., 2020; Liu et al., 2018; Thompson et al., 2022), while mean annual temperature reconstructions based on sea surface and terrestrial fossil records can be

---

biased because the proxies may actually indicate summer temperature changes (Bova et al., 2021; Mann et al., 2009a; Marsicek et al., 2018). Therefore, high-quality quantitative reconstructed records that can distinguish seasonal temperature change in different regions are strongly required.

Pollen-based quantitative reconstruction is crucial for connecting fossil records and simulations. The monsoon region in China, with its strong seasonality in climate and sensitive vegetation response, is ideal for the study of seasonal temperature change (Herzschuh et al., 2019; Zhou et al., 2016; Ran and Feng, 2013; Zhao and Yu, 2012; Chen et al., 2008; An et al., 2000). However, the existing pollen-based paleoclimate records in China are mostly qualitative and this lack of systematic quantitative reconstruction results (Zhao, 2018) hinders a better understanding of the spatial patterns and mechanisms of Holocene climate. Northeast China, located at the northern margin of the East Asian monsoon region, is ideal to fill the data gap. Although different proxies such as biomarkers (Zheng et al., 2018; Zheng et al., 2017; Zhou et al., 2010), grain size (Li et al., 2017), and diatoms (Li et al., 2020; Ma et al., 2018) have been used to quantitatively reconstruct the Holocene climate change in Northeast China, these studies show inconsistent results for the transition from warm/cold to dry/wet conditions during the Holocene. This discrepancy can be attributed to multiple factors, including differences in sample resolution, in spatial representation of the studied proxies, and in the sensibilities of seasonal change. Pollen, as a widely used proxy for regional vegetation, has shown its great potential for reconstructions of seasonal temperatures in temperate regions (Liang et al., 2020; Liu et al., 2019; Stebich et al., 2015; Wang et al., 2019). However, pollen-based quantitative reconstruction research, which uses the most common proxy and provides spatio-temporal comparison, is still inadequate (Stebich et al., 2015; Wu et al., 2016; Zhou et al., 2016).

The existing modern pollen database in China lacks boreal analogs and only a few quantitative reconstructions from high-resolution records can cover the Holocene, much less the study of seasonal change in Northeast China. Synthesized climatic series to study regional trends and features are also lacking. Therefore, a better modern pollen database and chronologically controlled, high-resolution pollen records in Northeast China are necessary.

Here, we present the results of a quantitative climate reconstruction based on a new high-resolution fossil pollen record from Gushantun (GST) peatland, Changbai Mountains and the synthesized climatic series of three pollen records in the eastern part of Northeast China. The main objectives of this study are: 1) to reconstruct the history of seasonal temperature change in Northeast China during the Holocene based on a richer database complemented by our newly obtained surface samples in Northeast China and Siberia, 2) to acquire synthesized climatic series and investigate regional features and drivers, and 3) to provide regional evidence to address the alleged seasonal bias of annual temperature reconstructions in the debate of the Holocene Temperature Conundrum.

2. Study region

The GST peatland (42.31° N, 126.28° E) is located on the western flank of Changbai Mountains at an elevation of 517 m a.s.l. and is nearly circular with a diameter from 800 m to 1000 m (Fig. 1). The peatland originates from a crater lake and contains a sedimentary deposit since the last deglaciation with a maximum thickness of 9 m (Leng, 2019; Liu, 1989; Zheng et al., 2018). Mean annual precipitation (MAP) at nearby Jingyu meteorological station (at 570 m a.s.l.) is 780 mm for the period 1981–2010. Most precipitation falls as rain in summer. Mean annual temperature (MAT) is ~3.8 °C, while mean temperatures of the coldest
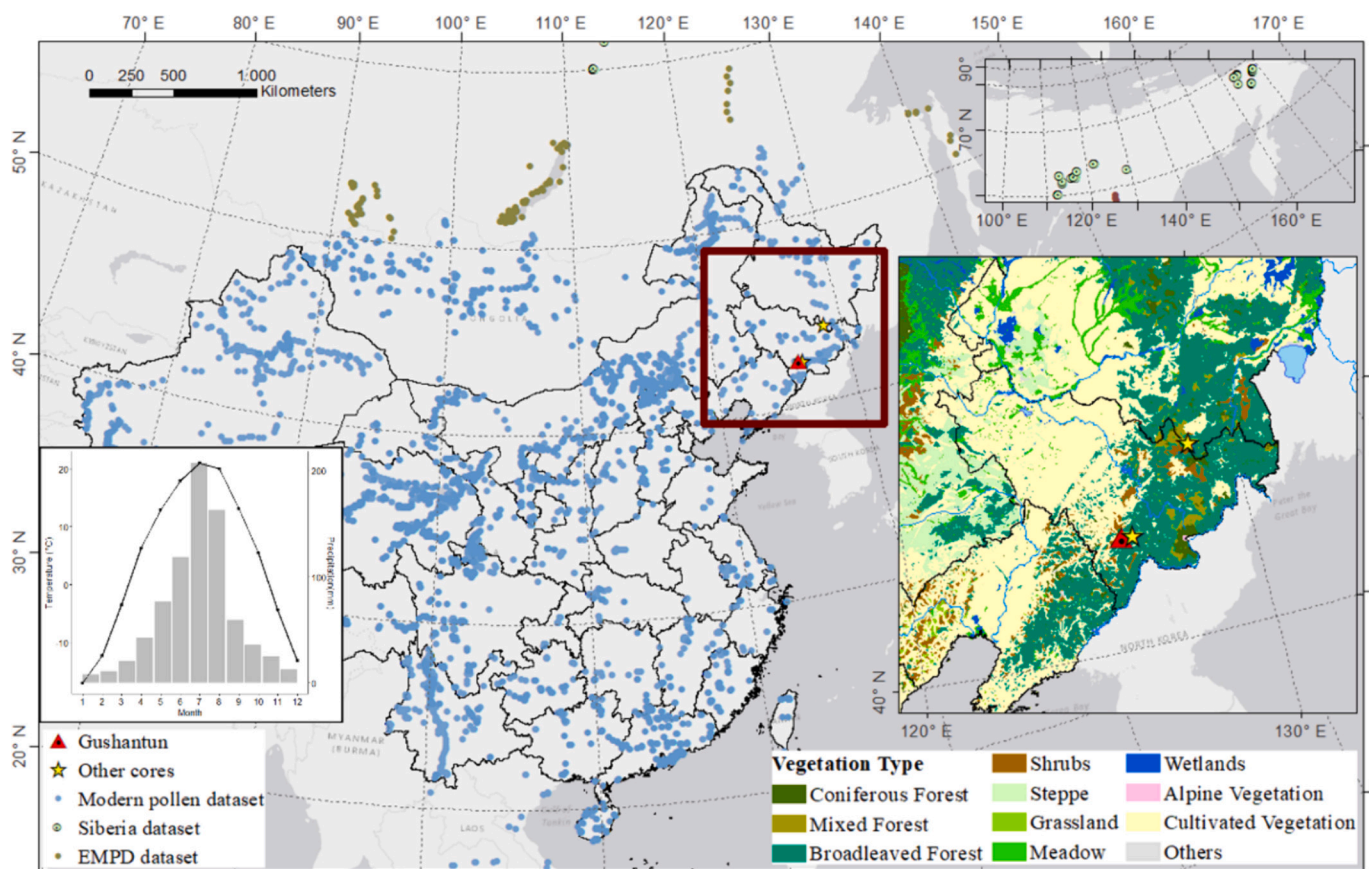

Fig. 1. Location of the fossil pollen records (red triangle and yellow stars) and modern pollen datasets. The large inset shows the vegetation map of the marked area (Hou, 2001). Monthly climate of the fossil record sampling site is also shown. (For interpretation of the references to colour in this figure legend, the reader is referred to the web version of this article.)

and warmest month are −17 °C and 21 °C, respectively.

The current vegetation at the vicinity of the GST sampling site is cultivated lands while the regional vegetation in the eastern part of Northeast China is composed of various forests including coniferous forest, mixed forest, and broadleaved forest. The coniferous forest is dominated by conifers such as *Larix*, *Pinus*, *Picea*, and *Abies*, while the mixed forest is dominated by both coniferous (*Pinus*, *Picea*, *Abies*) and broadleaved (*Betula*, *Tilia*, *Ulmus*, *Acer*, *Populus*, *Quercus*, *Fraxinus*, *Phellodendron*) trees. The broadleaved forest in Northeast China is mostly secondary vegetation; consequently, the composition of this type of forest is complex and diverse (Zhou, 1997).

3. Materials and Methods

3.1. Modern pollen dataset

The modern pollen datasets used in this study comprise 4356 samples in total (Fig. 1), including previously published (Cui et al., 2019; Davis et al., 2020; Geng et al., 2022; Geng et al., 2019; Herzschuh et al., 2019; Ma et al., 2017; Zhao et al., 2021; Zheng et al., 2014) and new data (not yet published). Samples from a Siberia dataset (Geng et al., 2022) and a subset of the European Modern Pollen Database (EMPD, Davis et al., 2020) were added as a supplement of boreal analogs in colder environments.

Climate data from 756 meteorological stations in the past thirty years (1981–2010) were derived from the China Meteorological Administration (http://data.cma.cn) and the mean climatic variables for each site of modern pollen samples were interpolated by thin plate spline regression. MAP, mean precipitation of the warmest month (Mpwa) and coldest month (Mpco), MAT, mean temperature of the warmest month (Mtwa) and coldest month (Mtco) were selected for the following analyses. MAT ranges from a minimum of −14.3 °C to a maximum of 36.8 °C (mainly distributed between −6 and 26 °C) while Mtco (mainly below 20 °C) and Mtwa (mainly 5–30 °C) also span a wide range. MAP has a relatively even distribution ranging from a minimum of 8 mm to a maximum of 2170 mm. This modern pollen dataset covers a wide range of climatic conditions which is the pillar of quantitative reconstruction (Fig. S1).

3.2. Sample collection and dating

The GST peat core was obtained with a Russian peat borer from the Gushantun peatland (Fig. 1) in the summer of 2017. The sediment core was 5.19 m long and subsampled at 1 cm intervals. A total of 249 pollen samples were processed and identified at 2 cm intervals. To meet the requirement for a high-resolution record, the terrestrial plant remains (plant leaves, seeds and charcoals, etc.) in 18 samples at appropriate depths were selected and used for accelerator mass spectrometry (AMS) radiocarbon dating at Beta Analytic Lab, USA (Table 1). All the radiocarbon ages were calibrated into calendar ages before present (BP) with the IntCal13 calibration curve (Reimer et al., 2013) while using the Bayesian age-depth model in rbacon package (Blaauw et al., 2021) from R.

3.3. Pollen analysis

The pollen samples ($n = 249$) were weighed and a known quantity of *Lycopodium* spores was added to approximate 1–2 g of peat lumps for the estimation of pollen concentrations (Stockmarr, 1971). Each sample was sieved to remove impurities and was processed following a modified acetolysis procedure (Faegri et al., 2000) which included HCl, NaOH, HF, and acetolysis treatments. The residue was then sieved through a 10 μm mesh and stored in liquid glycerin. At least 500 terrestrial pollen grains per sample were counted and identified at 40 × 10 magnification under a microscope. Pollen was identified using published pollen atlases and identification keys (Tang et al., 2016; Wang, 1995), plus a reference

Table 1
AMS ^{14}C dating results of Gushantun (GST) peat core from Beta Analytic Lab.

Depth (cm)	Material	Conventional Age	Calibrated Age	δ^{13}C (‰)
26	plant remains	90 ± 30 yr BP	156	−25
35	plant remains	70 ± 30 yr BP	234	−26.3
70	plant remains	1050 ± 30 yr BP	920	−24.2
81	plant remains	1090 ± 30 yr BP	1015	−26.9
107	plant remains	1340 ± 30 yr BP	1290	−29.5
127	plant remains	1840 ± 30 yr BP	1742	−24.9
149	plant remains	2050 ± 30 yr BP	2052	−27.7
167	plant remains	2410 ± 30 yr BP	2454	−27.5
194	plant remains	2990 ± 30 yr BP	3141	−28.1
210	plant remains	3190 ± 30 yr BP	3417	−27.3
235	plant remains	3600 ± 30 yr BP	3891	−27.4
255	plant remains	3790 ± 30 yr BP	4187	−23.1
283	plant remains	4130 ± 30 yr BP	4650	−22.6
327	plant remains	4550 ± 30 yr BP	5339	−25.6
366	plant remains	6210 ± 30 yr BP	7094	−25.3
408	plant remains	7600 ± 30 yr BP	8395	−26.2
446	plant remains	8240 ± 30 yr BP	9149	−27.9
493	plant remains	8640 ± 40 yr BP	9703	−22.1

collection of pollen from plants collected in the study area. Pollen percentages were calculated based on the total number of terrestrial pollen grains. A square root transformation of the pollen data was performed before all pollen-based statistical analyses and reconstructions.

3.4. Climate reconstruction

We followed a comprehensive framework for the climate reconstruction in this study (Liang et al., 2020; Zhao et al., 2021) encompassing modern pollen dataset screening, climatic variables, calibration set and reconstruction model selection, and evaluation and validation of the results. Taxa comprising >1% in at least one sample were selected as the input data. The reconstruction models including Modern Analogue Technique (MAT), Weighted Average (WA), Weighted Averaging Partial Least Squares (WAPLS), Locally Weighted Weighted Averaging (LWWA), and Locally Weighted Weighted Averaging-Partial Least Squares Regression (LWWAPLS) were run with different parameters. A significance test was conducted to assess the statistical performance of the reconstruction (Telford and Birks, 2011). Random reconstructions ($n = 999$) were derived from the same model trained on randomized data and the proportion of variance explained by these random reconstructions was estimated using redundancy analysis (RDA). A reconstruction is considered statistically significant if it explains more of the variance in the fossil data than most (95% by convention) random reconstructions. All the reconstructions and tests were conducted using the rioja (Juggins, 2022), analogue (Simpson et al., 2021), and palaeoSig (Telford and Trachsel, 2019) packages in R (R Core Team, 2019).

3.5. Data analysis

Hierarchical clustering and k-means clustering were used to analyze the modern and fossil pollen data. Ordination analyses were applied to investigate the relationships between pollen data and climate variables using the vegan package (Oksanen et al., 2019) in R. A detrended correspondence analysis (DCA) was initially performed to estimate the underlying linearity of the data. According to the results of the DCA, the gradient length of the first axis of the modern training dataset and the fossil pollen dataset are 3.2 and 1.3 standard deviation units, respectively. Consequently, the linear method of principal component analysis (PCA) was selected to assess the fossil pollen dataset, RDA was used in the significance test, and the unimodal method of canonical correlation analysis (CCA) was employed in the time-track analysis to access the relationship between the larger modern pollen and climate datasets. Boosted regression trees (BRT) analysis was performed to explore the relationship between climate variables and the modern pollen dataset using the gbm package (Greenwell et al., 2022) in R. The parameters

were adjusted based on pollen data so that the number of regression trees was >5000 and the model stability was guaranteed by repeating the calculation five times.

REDFIT (Schulz and Mudelsee, 2002) and the Morlet wavelet transform spectral analyses were conducted to investigate the periodicity of Holocene climate change. Prior to the spectral analyses, the reconstructed time series was detrended using the astrochron package in R (Meyers et al., 2021). The input data of the REDFIT method can be unevenly spaced time series and the output is the frequency and red-noise power spectrum curves. The result was assessed by a Monte Carlo simulation and false-alarm levels (90%, 95%, 99%) were given. The Morlet wavelet transform requires evenly spaced time series, so the time series was first interpolated to 40-year intervals using the interp. dataset function from the rioja package (Juggins, 2022). Signal power is shown by colour. A significance level corresponding to $p = 0.05$ is plotted as a contour (Torrence and Compo, 1998). The spectral analyses were conducted using the dplR package (Bunn et al., 2021) in R and the PAST software (Hammer et al., 2001).

3.6. Synthesis of time series

To further explore the regional Holocene climate-change pattern and compare it with other regions, three fossil pollen records comprising two published records, Sihailongwan (SHLW) (Stebich et al., 2015) and Jingpohu (JPH) (Li et al., 2011) from northeast China, as well as our GST record, that cover the last 10 kyr were synthesized (Table 2). The original pollen and chronological data of the published records (Li et al., 2011; Stebich et al., 2015) were used under the climate reconstruction framework of this study. Temperature trends were extracted using a generalized additive model (GAM). Due to the different chronological resolutions of the time series, the Mtco sequences reconstructed from the three pollen records were interpolated at 50-year intervals for comparisons using the interp.dataset function from the rioja package (Juggins, 2022) in R, and the mean value of the interpolated series was then calculated for synthesis.

4. Results

4.1. GST pollen record

A total of 62 pollen and spore taxa were identified from the 249 samples from the GST peat core. The radiocarbon ages of the GST peat core are shown in Table 1. Most of the conventional ages from the AMS ^{14}C dating had an error of ± 30 yr BP and the age at the depth of 493 m had an error of ± 40 yr BP. The ages of each dating sample were calibrated using a Bayesian age-depth model and the record covers 10,179 cal yr BP with a high average resolution of 40 years per sample (Fig. 2). The main taxa including four coniferous trees, six broadleaved trees, and 12 shrubs and herbs are shown in Fig. 3. The pollen record is clustered into five zones according to the results of a CONISS analysis.

Zone 1 (10.2–9.5 ka BP) is dominated by broadleaved taxa including *Quercus* (average 23%), *Betula* (13%), *Ulmus* (8%), and *Juglans* (8%). Conifers such as *Pinus* (2%) are less abundant. Cyperaceae (22%) is the most abundant herb while *Artemisia* (9%) and Chenopodiaceae (1%)

Table 2
Information of the fossil pollen records used in this study.

Site Name	Lat (°N)	Long (°E)	Elevation (m)	Age (ka BP)	Number of samples	Reference
GST	42.31	126.28	517	10.2–0	249	This study
JPH	43.91	128.77	350	9.0–0	225	Li et al. (2011)
SHLW	42.28	126.6	797	12.0–0	205	Stebich et al. (2015)

GST-Gushantun, JPH-Jingpohu, SHLW-Sihailongwan.

gradually increase in variability.

Zone 2 (9.5–7.3 ka BP) is still dominated by *Quercus* (26%) and *Ulmus* (11%). *Betula* decreases to its minimum average of 4% of all zones. Conifers and herbs remain similar to zone 1. A unique feature of this zone is the high proportion of the fern Polypodiaceae.

Zone 3 (7.3–5.5 ka BP) is dominated by broadleaved taxa with *Betula* (30%) increasing drastically to a maximum of 80%. Consequently, *Quercus* (20%), *Ulmus* (7%), and *Juglans* (7%) as well as herbs including Cyperaceae (11%) and *Artemisia* (7%) decrease. Conifers remain low.

Zone 4 (5.5–1.6 ka BP) is characterized by increasing coniferous taxa such as *Pinus* (21%). The proportion of *Betula* (13%) is stable while other broadleaved taxa including *Quercus* (13%), *Juglans* (6%), and *Ulmus* (7%) decrease.

Zone 5 (1.6 ka to present) is dominated by coniferous taxa, with significant increases in *Pinus* (37%) and *Abies* (3%). Broadleaved taxa such as *Betula* (11%), *Quercus* (8%), *Ulmus* (4%), and *Juglans* (4%) are less abundant compared to zone 4. Ericaceae (2%) shrubs increase significantly while Cyperaceae herbs decrease to 12%.

The PCA explores the distribution of pollen data (taxa >1% in at least one sample). Broadleaved taxa such as *Quercus*, *Tilia*, *Juglans*, and *Ulmus*, which tend to grow in warmer southern areas, are distributed on the positive side of the first axis, whereas *Abies* and *Picea*, which are distributed on the negative side, tend to grow in cooler environments. The *Quercus/Betula* ratio (QB ratio) has a strong correlation with Mtco (Geng et al., 2019), while *Quercus* and *Betula* in the fossil pollen data also point in the positive and negative directions of the first two axes, respectively. In summary, the first axis of the PCA results probably indicates regional temperature change, with the positive direction indicating higher temperatures and vice versa (See details in Supplementary Materials).

4.2. Selection and assessment of quantitative reconstruction models

The BRT analysis determines the controlling climatic factors of the modern vegetation composition, while the time-track analysis investigates the similarity between fossil and modern pollen data over time by superimposing the fossil pollen data on the modern pollen ordination. The distribution of the time series along the climatic variables are observed to determine the dominant climate factor for vegetation change at long time scales (Birks et al., 2012). The results of both analyses (Fig. S3) show that temperature, especially Mtco, is the most important factor for the vegetation change in the study area while the abundant precipitation is not a limiting factor for tree growth. Therefore, MAT, MAP, Mtco, and Mtwa were selected for reconstruction.

In order to select the most appropriate reconstruction model for this study, five commonly used methods, MAT, WA, WAPLS, LWWA, and LWWAPLS, were used and compared (Table S1). The R^2 values range from 0.67 to 0.91, indicating that all these methods are statistically valid. Although MAT, LWWA, and LWWAPLS have smaller root mean squared errors (RMSEs) and higher R^2 values, they have considerably larger average bias compared to WA and WAPLS. MAT exhibits a spiky pattern (Fig. S4), which may reflect that a relatively small number of analogs were employed in the reconstructions. This could be an instance where our modern pollen dataset lacks sufficient boreal analogs at the northernmost edge. Given that LWWA and LWWAPLS, like MAT, also require an extensive training set of modern analogs, these three methods may not be the most suitable methods for this study. For the remaining models, WAPLS has a lower RMSE and a higher R^2 compared to WA. WA is also prone to having edge effects, while WAPLS, as an improved method of WA, extracts additional components to maximize covariance with climate variables and has better empirical predictive power (Birks et al., 2012).

Based on the analysis above, WAPLS, with its reasonable results and relatively smaller errors, was selected for reconstructions in the study area. Furthermore, the trend of the Mtco reconstructed by WAPLS is consistent with the QB ratio, which demonstrates the suitability of the
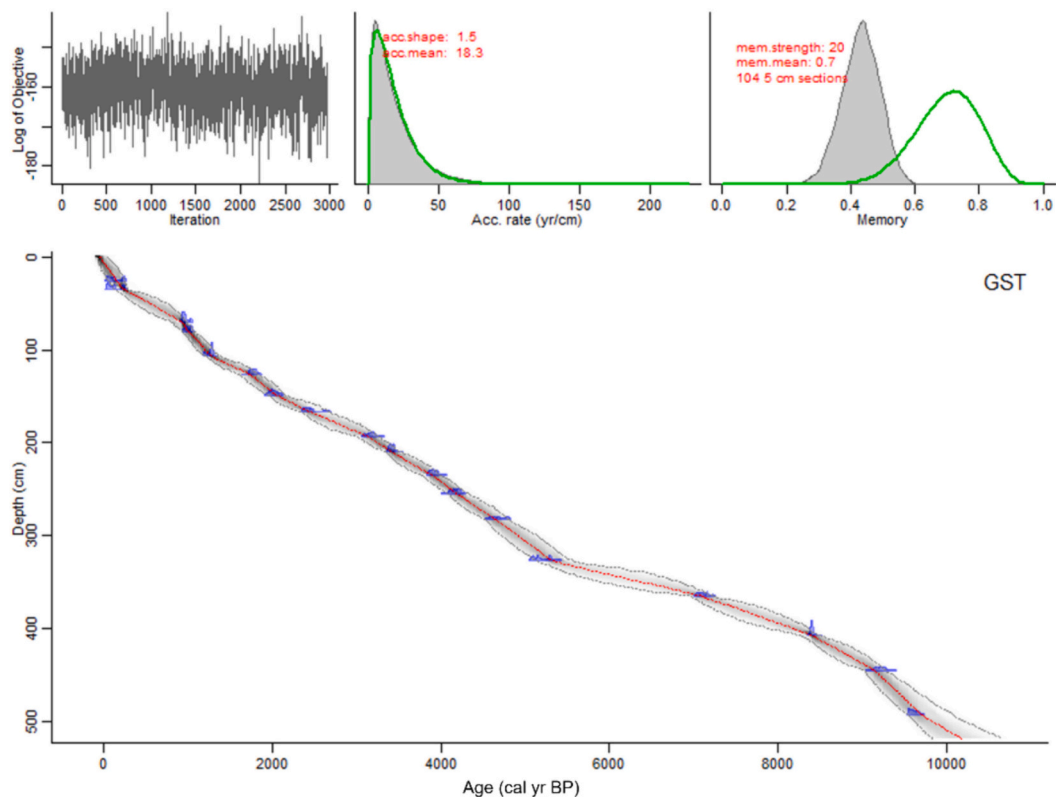
Fig. 2. Calibrated age-depth model of the Gushantun (GST) core established by a Bayesian model (Bacon; Blaauw et al., 2021). The radiocarbon ages were calibrated into calendar ages before present (cal yr BP) with the IntCal13 calibration curve. The grey area shows the 95% confidence interval.

WAPLS reconstruction.

The significance test was used to evaluate the reconstructions rather than just the model itself. In our case, reconstructed Mtco and MAT using WAPLS passed the significance test (Fig. S5), indicating that the temperature reconstructions for this peat core are more reliable than those with precipitation. This result is also consistent with the analysis of the controlling factors in the modern pollen dataset.

The two previously published pollen records, SHLW and JPH, were reanalyzed following the same procedures described above. The final method chosen for both records was also WAPLS, (Table S2).

4.3. Reconstructed climatic variables

The average Mtco during the Holocene is −17.2 °C (−22.9 °C ∼ −14.3 °C) and the moving averages of Mtco were calculated to remove the bias caused by extreme values, showing that the amplitude of Mtco is 4.7 °C (−19.6 °C ∼ −14.9 °C). The reconstruction result shows that the Megathermal occurred around 7–8 ka and the Mtco is 2 °C higher than in modern times (Fig. 4). Temperature decreases erratically from 5.6 ka, and cold events can be observed at 8.7, 7.8, 5.7, and 2.5 ka BP. Although MAP did not pass the significance test, it was still reconstructed and varies between 630 and 1000 mm, with significant decreases in precipitation as well as temperature between 9.4 and 8.5 ka BP (Fig. 4). Overall, the climate events for precipitation are not as significant as for temperature.

The QB ratio is an important indicator of the Mtco according to our previous research on the modern pollen-climate relationship in Northeast China (Geng et al., 2019). In this study, the reconstructed Mtco and MAP were compared with the QB ratio, and the coniferous and broad-leaved taxa content in the fossil pollen data (Fig. 4). The trend in Mtco change is generally consistent with the QB ratio in the fossil pollen data. The decrease in Mtco from 5.7 ka corresponds to an increase in *Betula* and coniferous taxa in the fossil pollen data. These comparisons

corroborate each other and support the reliability of the reconstruction result.

The results of the REDFIT analysis of Mtco (Fig. 5a) show that it had relatively significant 105- and 1200-year cycles. The results of the Morlet wavelet transform of the Mtco (Fig. 5b) show strong signals of an approximate 1500-year cycle during 8–1.5 ka BP and a 700- to 800-year cycle during 7.5–4.5 ka BP.

4.4. Synthesized series of multiple pollen records

The trends of the reconstructed climatic variables of the three selected records in this study are generally similar, and the dominant climatic factor is Mtco rather than precipitation. The Mtco reconstructions of JPH and GST are consistent in both absolute values and trends, while the reconstruction for SHLW is relatively high but with a similar trend (Fig. 6b).

The temperature variables reconstructed in this study include MAT, Mtco, and Mtwa, all of which are highly correlated, and Mtco was chosen as the main temperature indicator of the study area because the vegetation change in the eastern part of Northeast China is mainly controlled by winter temperature (Geng et al., 2019). The synthesis of Holocene temperature changes (Fig. 6a) shows that Mtco first decreases and then increases during the early Holocene.

A cold event is observed at ∼8.7 ka BP, probably corresponding to the 8.2 ka event considering the age uncertainty, after which the Megathermal occurred between 8 and 6 ka BP. Subsequently, the temperature decreases and cold events also occur around 5.7 ka BP and 2.5 ka BP, followed by a short-term rebound during 2.0–1.5 ka BP. The mean synthesized Mtco is −15.7 °C (−18.4 ∼ −13.2 °C) and the variation of the moving averages is 3.9 °C.
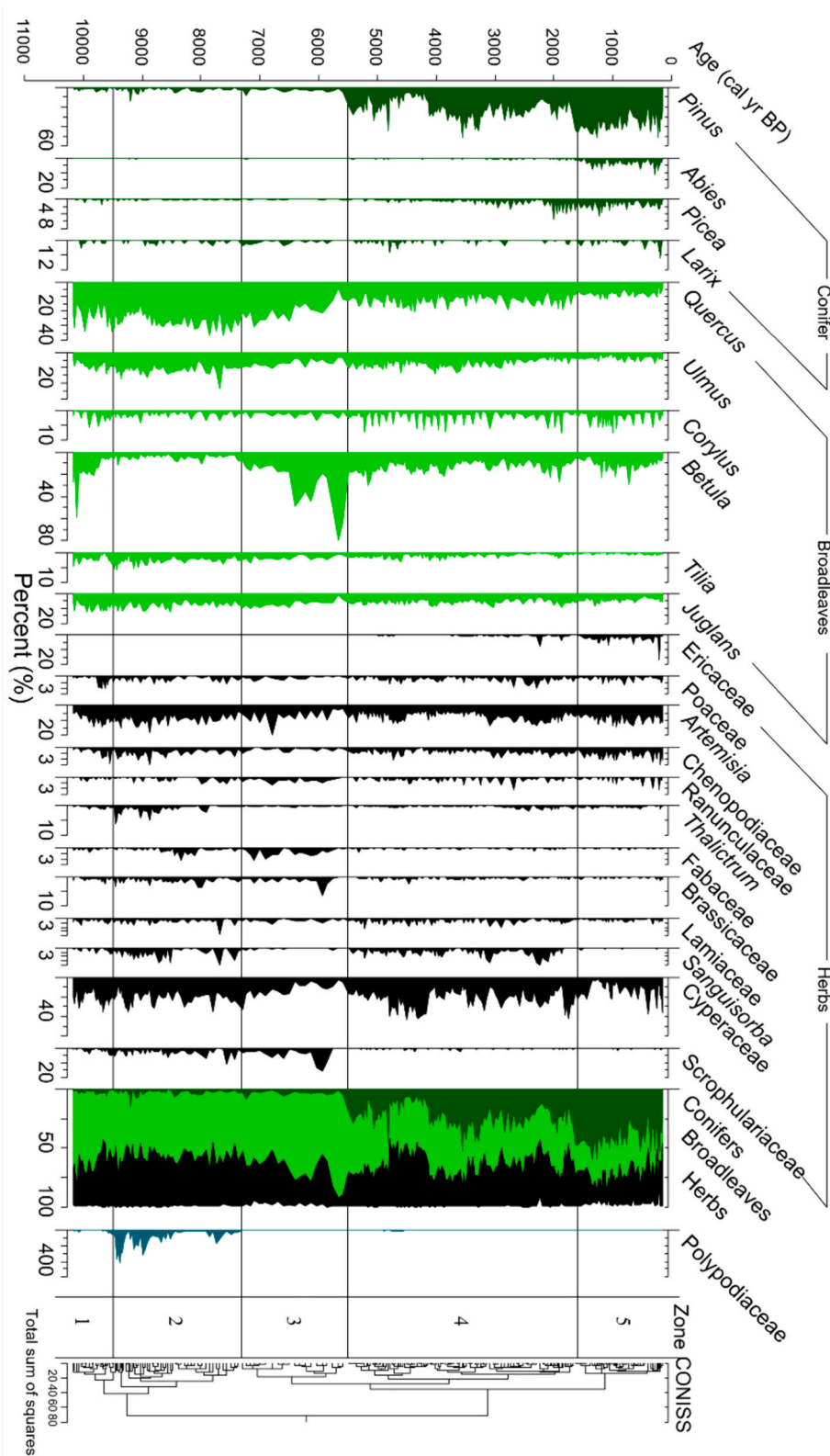
Fig. 3. Pollen diagram of the Gushantun (GST) peat core. The main taxa are grouped into conifers, broadleaves, and herbs. Each taxon, including Polypodiaceae, is divided by the terrestrial pollen sum and then calculated as a percentage. The result of the CONISS analysis is shown.

5. Discussion

### 5.1. Features of temperature changes in Northeast China

Comparison of the trends of the synthesized MAT and Mtco anomalies in the study area (Fig. 7a) shows that they are generally synchronous, but differ in amplitude in some time periods. They show a distinct Megathermal between 8 and 6 ka BP (Fig. 7a). Temperature increases until 7.2 ka, during which time MAT has a greater amplitude of variation than Mtco. After reaching their peaks (MAT peaks later), Mtco
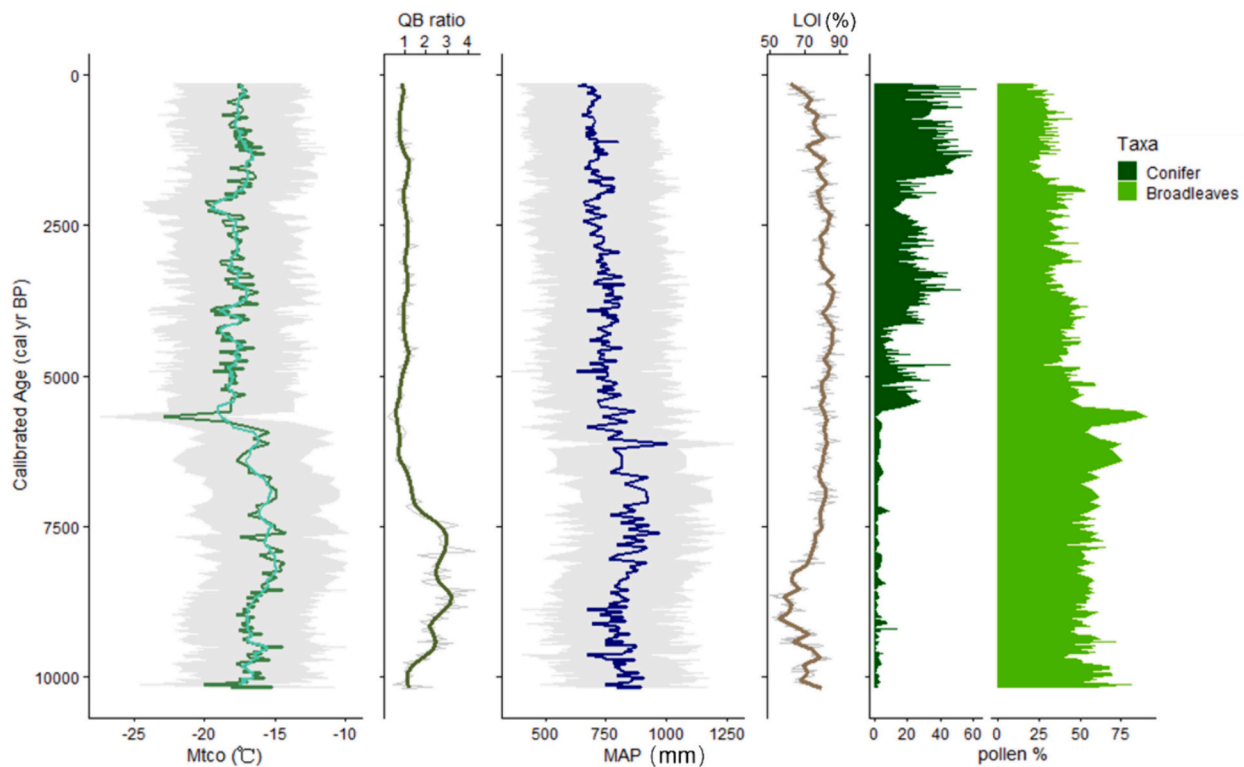
Fig. 4. Reconstructed climatic variables compared with other proxies (the light green line is the moving averages of mean temperature of the coldest month (Mtco), error is in grey, QB ratio = *Quercus/Betula* ratio, LOI = loss on ignition of organic matter) at the Gushantun (GST) site. Percentages of coniferous and broadleaved taxa content in the fossil pollen data are shown. (For interpretation of the references to colour in this figure legend, the reader is referred to the web version of this article.)
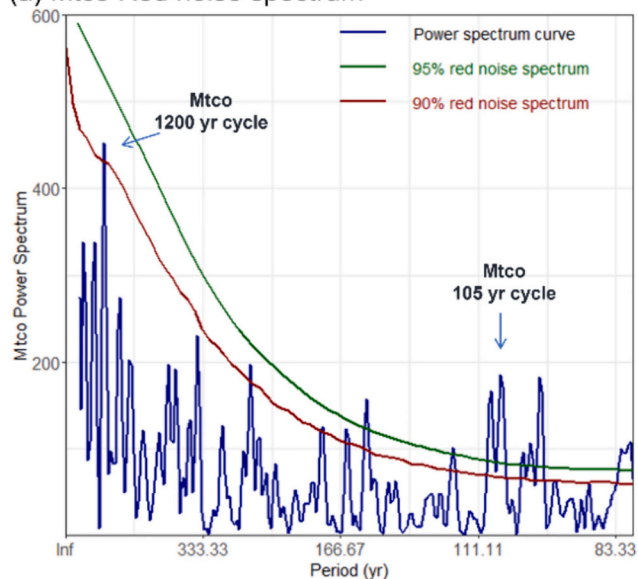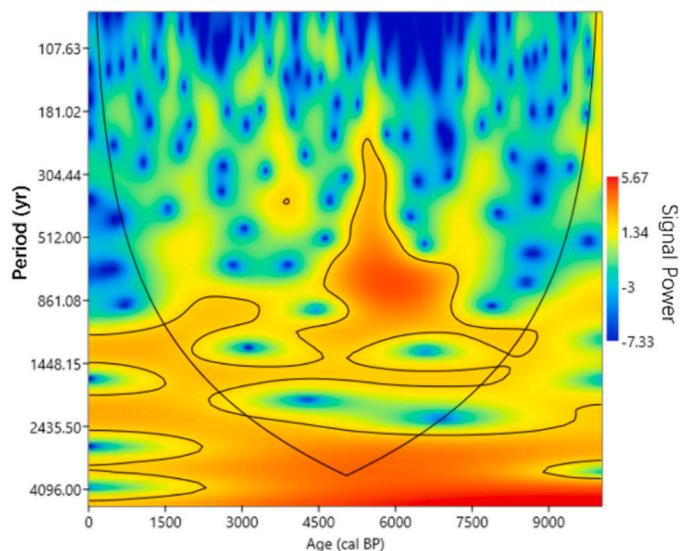

Fig. 5. The results of (a) REDFIT spectral analysis of the mean temperature of the coldest month (Mtco) (the 90% and 95% confidence levels are shown as colored lines), and (b) Morlet wavelet transformation of Mtco (black line is the 95% significant contour) reconstructed for the Gushantun (GST) site.

decreases more than MAT, while between 3.5 ka and 2.7 ka Mtco decreases less than MAT. Between 2.7 ka and 1.6 ka, Mtco increases slightly, while MAT remains on a decreasing trend. After 1.6 ka, Mtco starts to decrease again, but the decreasing amplitude is much smaller than the MAT.

We compared these pollen-based temperature curves with other proxies such as grain size, phytoliths, and biomarkers in the study area

(Fig. 7): they all show a consistent increasing and then decreasing trend albeit with minor variances due to differences in resolution, proxy, and chronological calibration. These multiple proxies corroborate each other, indicating that the Holocene temperature reconstructed from pollen records in Northeast China is reliable. Furthermore, although temperature curves show cold events at different times, they mainly occur during 8.8–8.5 ka BP, 7.8–7.5 ka BP, 6.0–5.5 ka BP, and 2.6–2.3 ka
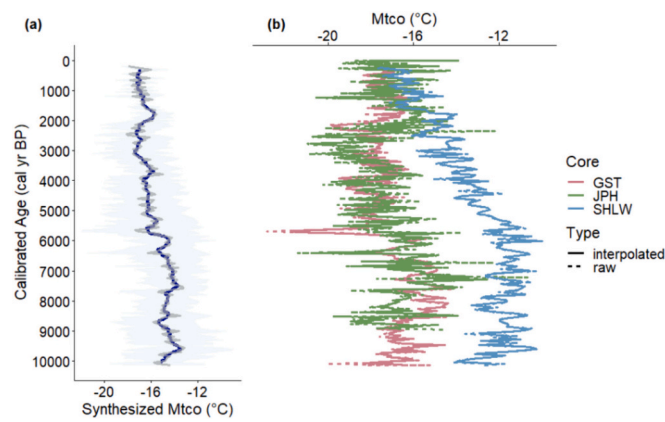
Fig. 6. Plots of (a) synthesized mean temperature of the coldest month (Mtco) (in grey, mean value of the interpolated Mtco of three records), its standard deviation (light blue area) and its moving average (in dark blue), and (b) the raw (dashed line) and interpolated (solid line) Mtco sequences of the three selected pollen records in northeast China. (For interpretation of the references to colour in this figure legend, the reader is referred to the web version of this article.)

BP, with a regular 3 ka interval corresponding to the strong signal of the 1.5 ka cycle in the spectral analysis.

Comparison with pollen-based quantitative reconstructions from other regions of China (Fig. 8a-c) shows a consistent decreasing trend during the Holocene as well as the climate events, especially the 8.2 ka cold event, with different amplitudes and onset times. We compared our reconstruction with oxygen isotope records that can indicate the local East Asian monsoon and the temperature anomaly in the Northern Hemisphere (Fig. 8d-f). The multi-indicator comparison also shows that the Holocene climate change in China has a consistent general decreasing trend with different amplitudes and onset of the Megathermal. The Holocene Megathermal recorded in the eastern monsoon

region is significantly earlier, peaking between 8 and 7 ka BP, while the Tibetan Plateau record peaks at around 5 ka BP (Liang et al., 2020) and the more northern Siberian region is suggested to have a Holocene Megathermal between 6 and 4.5 ka BP (Andreev et al., 2001), which are much later than the East Asian monsoon region.

In addition to the trend, most of the reconstructed sequences show prominent cold events between 9 and 7.5 ka BP. The 4.2 ka event was not found in the temperature sequences in Northeast China, while cold events were more pronounced around 6.0–5.5 ka BP and 3.0–2.5 ka BP with larger amplitudes, suggesting that the form and intensity of cold events varies from region to region. Zheng et al. (2016) conclude that the Tibetan Plateau has a lower MAT with smaller amplitude (Herzschuh et al., 2014), while MAT in the eastern monsoon region has a maximum amplitude of up to 15 °C (Tarasov et al., 2011; Yoshida and Takeuti, 2009). Zheng et al. (2017) also suggest that the amplitude of temperature change may be larger at higher latitudes. The paleoclimate simulation results from Liu et al. (2009) corroborate this opinion with a greater temperature change in Northeast China than in other lower latitude regions.

### 5.2. Seasonal temperature change and its implication for the Holocene Temperature Conundrum

As a direct record of vegetation, pollen data can better reconstruct the dominant controlling factors such as seasonal temperature or precipitation. Liang et al. (2020) analyzed pollen records from the eastern Tibetan Plateau to demonstrate that the dominant controlling factor for vegetation change in their study area is Mtwa. For pollen records from other regions such as the Dajiuhu peat in the Shennongjia Mountains of central China, Sun et al. (2019) suggest that they mainly reflect the local precipitation controlled by the East Asian monsoon. Therefore, pollen records from different regions reflect the main factor influencing the vegetation changes.

One possible explanation for the Holocene Temperature Conundrum lies in the different sensitivity of the different proxies to temperature seasonality or climate patterns in different regions. Ecologically, the
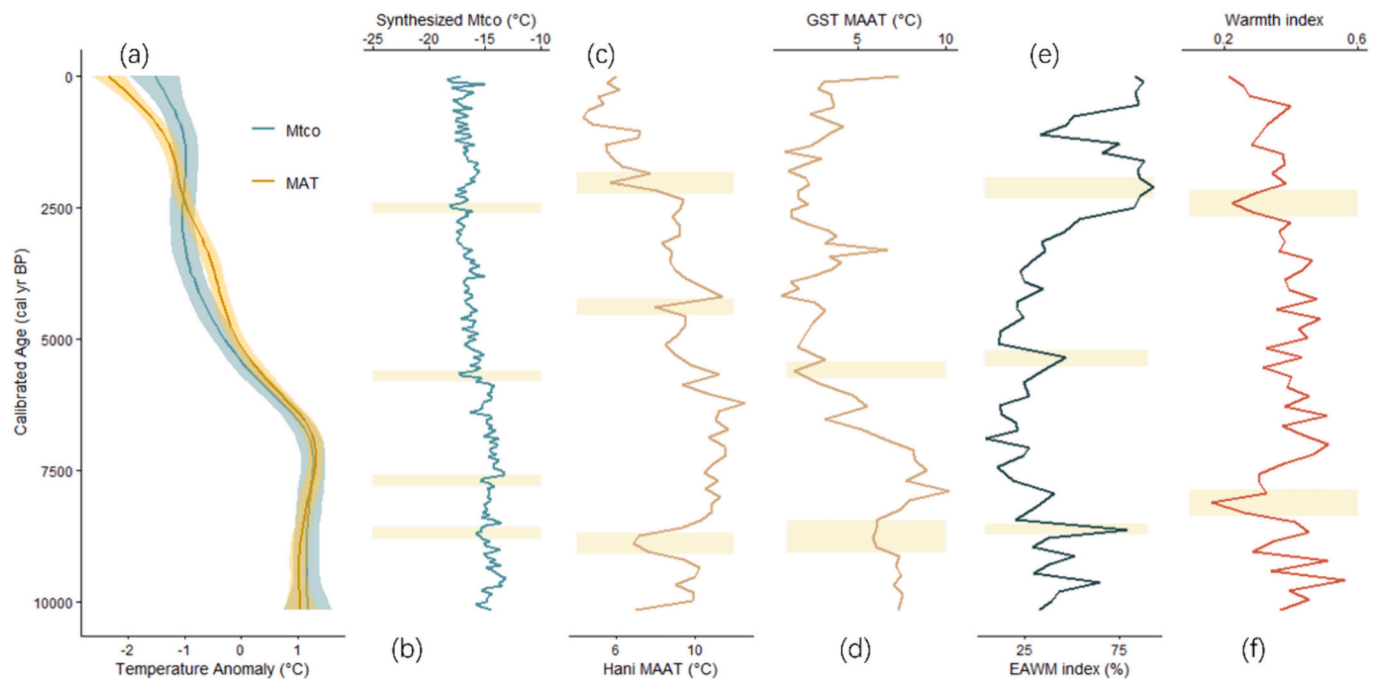
Fig. 7. Comparison of pollen-based reconstructed temperature series and other proxies. (a) Trends of synthesized mean annual temperature (MAT) and mean temperature of the coldest month (Mtco) anomaly in NE China (colored area is 95% confidence interval), (b) Synthesized Mtco, (c) branched glycerol dialkyl glycerol tetraethers (brGDGTs)-based MAT in Hani (Zheng et al., 2018), (d) brGDGTs-based MAT in Gushantun (GST) (Zheng et al., 2018), (e) index of East Asian winter monsoon based on grain size (Li et al., 2017), (f) Phytolith-based warm index in Gushantun (Gao et al., 2018).
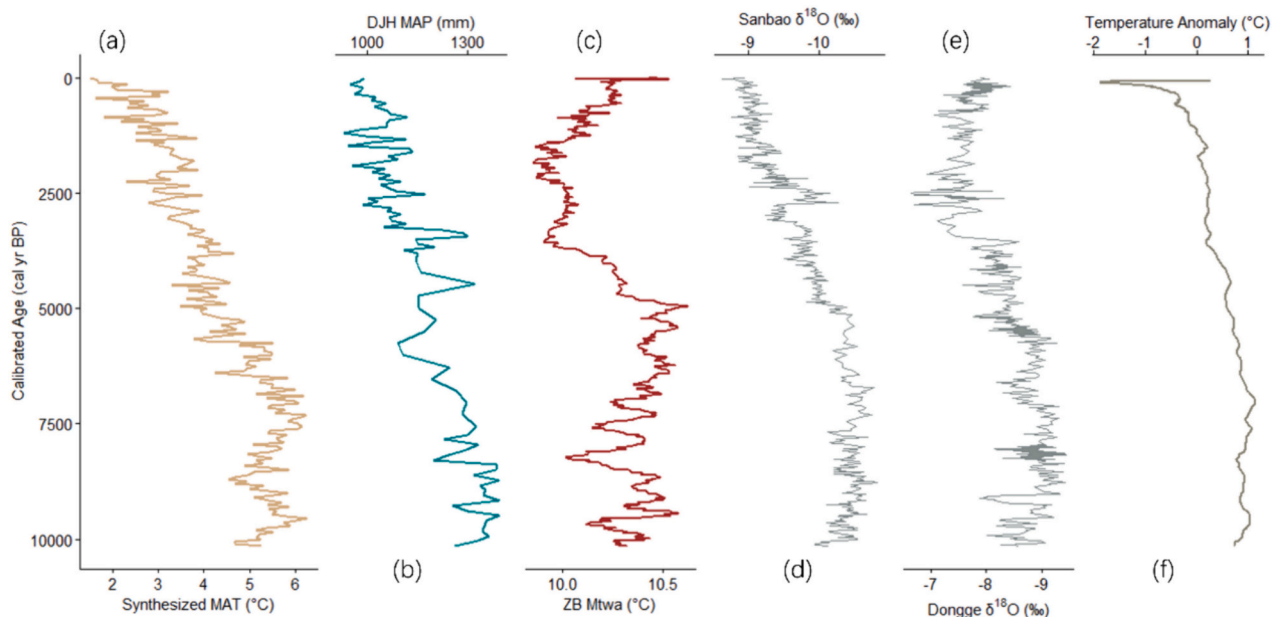
Fig. 8. Reconstruction results from different proxies and regions. (a) Synthesized mean annual temperature (MAT) in NE China from this research, (b) mean annual precipitation (MAP) from Dajiuhu (Sun et al., 2019), (c) synthesized mean temperature of the warmest month (Mtwa) of eastern Tibetan Plateau (Liang et al., 2020), (d) stalagmite oxygen isotope results from Sanbao cave (Wang et al., 2008), (e) stalagmite oxygen isotope results from Dongge cave (Dykoski et al., 2005), (f) regional temperature anomaly for 90–30°N (Marcott et al., 2013).

variation in precipitation has a less fundamental impact on vegetation change than temperature does in the eastern part of Northeast China because precipitation is not the dominant growth-limiting factor once it exceeds the minimum requirement for the forests (Geng et al., 2019). Temperature, especially Mtco, shapes the structure of forests in Northeast China. The highly consistent relationship between QB ratio and Mtco (Fig. 3) corroborates this conclusion.

In contrast to the proxy-based reconstructions, climate model simulations suggest a gradual increase in Holocene temperature. Even after accounting for seasonal biases in the model, the simulated cooling amplitude is only half that of the reconstructed fossil record (Liu et al., 2014). Mann et al. (2009a, 2009b) suggest that proxy-based temperatures at mid- to high-latitudes in the Northern Hemisphere may be more biased towards surface temperatures in warm seasons during the early to mid-Holocene. However, Zhang et al. (2017) compared simulations and records from high latitudes in the Northern Hemisphere and conclude that some areas in the Northern Hemisphere (Greenland, Canada, Northern Europe) show a trend from early-Holocene warming to mid- to late-Holocene cooling in both simulations and fossil records.

According to the syntheses of the Holocene Mtco and MAT in this study, both temperature series exhibit a consistent decreasing trend from the mid- to late Holocene, indicating that the decreasing MAT trend in Northeast China is not biased by summer temperature. A similar pattern has been revealed in other pollen-based temperature reconstructions (Wen et al., 2013; Xu et al., 2010), which opposes the Holocene long-term warming trend from climate simulations and the seasonal bias explanation. Wu et al. (2023) suggest that records exhibit a consistent pattern with a warmer mid-Holocene and colder late Holocene in the Asian summer monsoon (ASM) domain, whilst records show a colder mid-Holocene and warmer late Holocene in the westerlies domain. The latest study from Kaufman and Broadman (2023) also suggests that a relatively mild millennial-scale global thermal maximum can be found in several compilations of globally distributed terrestrial and marine proxy datasets.

5.3. Possible driving factors

Solar radiation is the most direct external factor influencing surface

temperature, and can also indirectly influence atmospheric circulation through thermal differences between regions (Kaboth-Bahr et al., 2021; Kang et al., 2018; Kaufman and Broadman, 2023). The MAT trend reconstructed in this study is consistent with the summer insolation at the same latitude (Fig. 9f). Both the temperature and insolation peak during the early Holocene and gradually decrease during the mid- and late Holocene. Although both MAT and Mtco decrease during the mid- and late Holocene, MAT decreases more while Mtco has a flat and even slightly increasing phase between 2.7 ka and 1.6 ka BP (Fig. 7a). This discrepancy may be due to the increase of solar radiation in the coldest month (Fig. 9f). In addition, Mtco can be influenced by coupled atmospheric circulation patterns and mechanisms (Kaboth-Bahr et al., 2021; Wassenburg et al., 2016; Zhang et al., 2022). The summer insolation may be the initial driver of climate change in mid-latitude East Asia, via ice-sheet effects, monsoon circulation, atmospheric dust, and vegetation (Bader et al., 2020; Dong et al., 2022; Liu et al., 2018; Thompson et al., 2022).

Dong et al. (2022) propose that seasonal temperature does not simply respond to winter and summer insolation as predicted by climate models. Another important controlling factor for Northeast China is the East Asian monsoon. The cooling trend during the mid- to late Holocene is primarily controlled by the persistent weakening of the warming effect of the East Asian Summer Monsoon (EASM) and the concurrent strengthening of the cooling effect of the East Asian Winter Monsoon (EAWM; Wu et al., 2023). Comparing the reconstructed Mtco (Fig. 7b) with the EAWM index (Fig. 7e) based on grain-size analysis (Li et al., 2017), the trends of both are consistent. The EAWM is weaker in the early to mid- Holocene, corresponding to the Holocene Megathermal, and becomes stronger in the late Holocene, corresponding well to the increasing Mtco. Not only are the trends consistent, but the cold events also correspond to peaks in the EAWM index. Therefore, the EAWM plays a crucial role in the Mtco change.

The North Atlantic Oscillation (NAO) and the Arctic Oscillation (AO) can also influence Holocene temperature changes in China via teleconnection patterns (He et al., 2017; Pei et al., 2019; Zuo et al., 2015). Atlantic Meridional Overturning Circulation (AMOC) and Asian summer monsoon circulation are closely coupled (Cheng et al., 2016; Zhang et al., 2019). A positive-phase AO can cause a relatively weaker EAWM
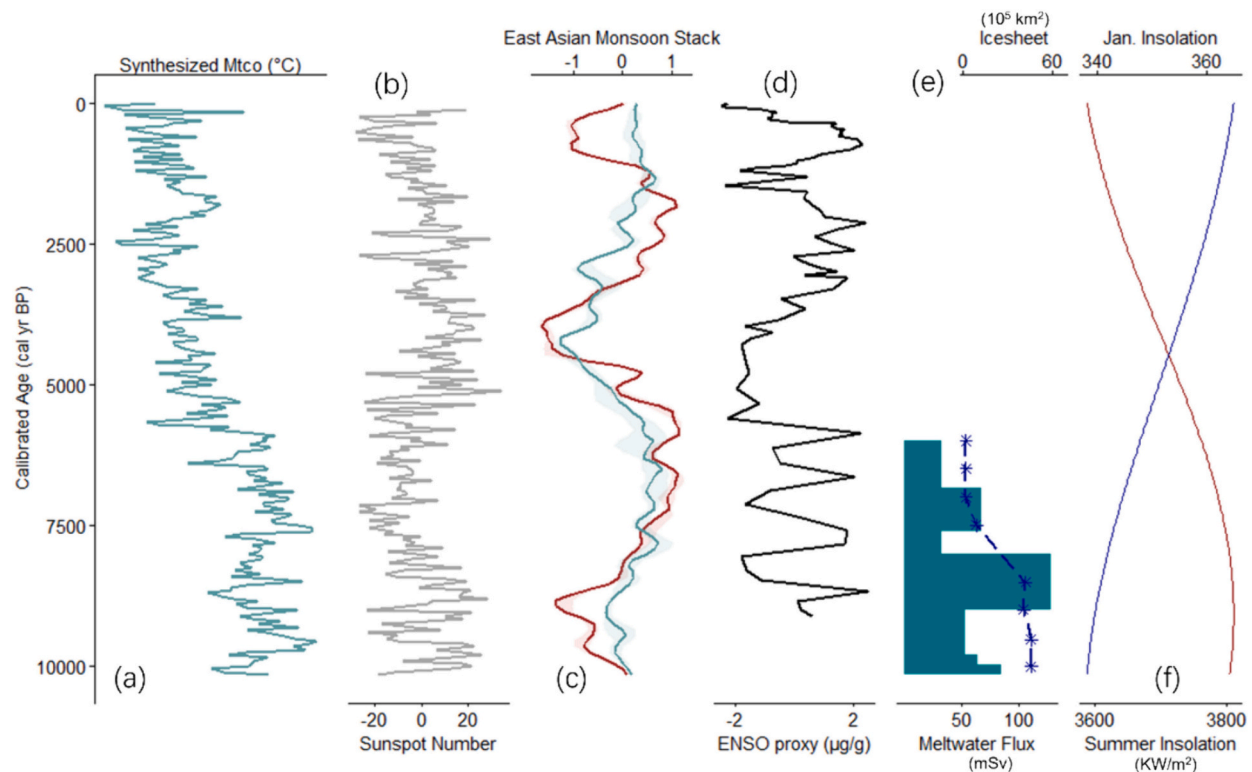
Fig. 9. Comparison of synthesized mean temperature of the coldest month (Mtco) and driving mechanisms. (a) Synthesized Mtco in this study, (b) detrended variation of sunspot number (Solanki et al., 2004), (c) East Asian summer monsoon (in red) and winter monsoon (in blue) stacks with 1 σ uncertainty (Kaboth-Bahr et al., 2021), (d) proxy for El Niño-Southern Oscillation (ENSO), concentrations of botryococcenes on a log scale (Zhang et al., 2014), (e) ice-sheet area (cyan histogram, 10⁵ km²) and meltwater flux (dark-blue line, mSv) (Zhang et al., 2018), (f) 45°N insolation (KW/m², summer in red, coldest month in blue) (Berger et al., 2010). (For interpretation of the references to colour in this figure legend, the reader is referred to the web version of this article.)

with higher winter temperatures. Zheng et al. (2017) suggest that the relatively larger amplitude of temperature change in Northeast China compared to other regions may be caused by the teleconnection from higher latitudes. Thus, climate change in the North Atlantic may have a strong influence on the northern part of the East Asian monsoon region.

Referring to the cold events summarized by Bond et al. (2001), the events observed in this study in Northeast China may correspond to the 8.2 ka BP, 5.9 ka BP, and 2.8 ka BP cold events. The wavelet analysis shows a 1500-yr cycle with a strong signal in the study area, which may correspond to these cold events. The study from Xu et al. (2019) reveals a ~ 500-yr periodic EASM oscillation in Northeast China during the Holocene, which can be one of the factors influencing the events. These cold events may also be influenced by the changes in the AMOC, Arctic sea-ice cover, El Niño-Southern Oscillation (ENSO), and sunspot activity (Kaboth-Bahr et al., 2021).

The cold events recorded in Northeast China are not contemporaneous with those summarized by Bond, with the most pronounced cold event in the record occurring at 8.8–8.6 ka BP rather than 8.2 ka BP, but correspond to the peak in meltwater flux since 10 ka (Fig. 9e). Thus, the change in the AMOC due to the massive meltwater flux may be the main cause of this cold event in Northeast China. The 5.8–5.5 ka BP cold event occurs during the transition period from a warm-wet to a cold-dry climate in the study area, with a decrease in solar radiation at low latitudes and a significant decrease in ESAM intensity (Fig. 9c). Moreover, sunspot activity fluctuates dramatically with a significant peak (Fig. 9b) and ENSO becomes weak between 5.6 and 5.2 ka BP (Fig. 9d). Therefore, it is likely that this event is not only driven by the AMOC but also by a combination of solar radiation, sunspot activity, and ENSO.

A 700 to 800-yr cycle between 7.5 and 4.5 ka BP is observed in the spectral analysis, which corresponds to an 800-yr cycle observed in North Atlantic and Arctic climate-change studies (Darby et al., 2017;

Turney et al., 2005) and in the Loess Plateau monsoon record (Kang et al., 2018). The decreasing amplitude of MAT also becomes smaller than that of Mtco during this phase. Therefore, this 800-yr cycle may be influenced by a combination of solar radiation, East Asian monsoon, and AMOC, etc. The end of this cycle is also consistent with a shift in East Asian monsoon phases as suggested by Kaboth-Bahr et al. (2021), which may be triggered by the decreasing insolation at low latitudes that reached a threshold at 4.5 ka BP.

6. Conclusion

The seasonal temperature change of the study area during the Holocene was reconstructed using high-resolution fossil pollen records with precise chronological control, and the characteristics and driving mechanisms of temperature change in Northeast China were discussed. The trends of MAT and Mtco in the Changbai Mountains are highly correlated. Inferred Mtco during the Holocene Megathermal reached a maximum of −14.5 °C in the early Holocene, which is about 2.5 °C warmer than the modern temperature, and gradually cooled in the late Holocene to a minimum of −19.6 °C. Four prominent cold events occurring around 8.7 ka BP, 7.8 ka BP, 5.7 ka BP, and 2.5 ka BP with an amplitude variation of up to 3 °C were revealed. A 1500-yr cycle of temperature change was also found. Furthermore, synthesized temperature series based on multiple pollen records showed the temporal and spatial characteristics of seasonal temperature change in Northeast China by comparing them with other proxies and regions. MAT decreased more than Mtco, but both showed a consistent decreasing trend during the mid- and late Holocene, indicating that the decreasing trend of MAT in Northeast China was not a bias caused by summer temperature.

Regional and global comparisons showed that solar radiation was the

most direct external influence on temperature change. The decreasing trend of Mtco was different from the existing simulation results and winter insolation. It was apparently under the influence of the EAWM since the cold events occurred with an enhanced winter monsoon. The 1500-yr cycle of climate change was consistent with the cycle of Bond events, which may be driven by a combination of forcing factors such as sunspot activity, AMOC, NAO, and AO. There was no significant reduction in arboreal pollen in the pollen records due to human activities in Northeast China, suggesting that the changes should mainly reflect natural climate change. However, human impact may still have been present and should be further analyzed.

Funding

CRediT authorship contribution statement

Rongwei Geng: Writing – original draft, Methodology, Investigation, Funding acquisition, Formal analysis, Conceptualization. **Yan Zhao:** Writing – review & editing, Supervision, Funding acquisition, Conceptualization. **Ulrike Herzschuh:** Writing – review & editing, Supervision. **Qiaoyu Cui:** Writing – review & editing. **Zhuo Zheng:** Writing – review & editing, Resources. **Xiayun Xiao:** Resources, Investigation. **Chunmei Ma:** Resources, Investigation. **Chen Liang:** Investigation, Formal analysis.

Declaration of competing interest

The authors declare that they have no known competing financial interests or personal relationships that could have appeared to influence the work reported in this article.

Data availability

Data will be made available on request.

Acknowledgments

Appendix A. Supplementary data

Supplementary data to this article can be found online at https://doi.org/10.1016/j.palaeo.2024.112391.

References

An, Z., Porter, S.C., Kutzbach, J.E., Xihao, W., Suming, W., Xiaodong, L., Xiaoqiang, L., Weijian, Z., 2000. Asynchronous Holocene optimum of the East Asian monsoon. Quat. Sci. Rev. 19, 743–762. https://doi.org/10.1016/S0277-3791(99)00031-1.

Andreev, A.A., Klimanov, V.A., Sulerzhitsky, L.D., 2001. Vegetation and climate history of the Yana River lowland, Russia, during the last 6400 yr. Quat. Sci. Rev., Beringian Paleoenvironments - Festschrift in Honour of D.M. Hopkins 20, 259–266. https://doi.org/10.1016/S0277-3791(00)00118-9.

Bader, J., Jungclaus, J., Krivova, N., Lorenz, S., Maycock, A., Raddatz, T., Schmidt, H., Toohey, M., Wu, C.-J., Claussen, M., 2020. Global temperature modes shed light on the Holocene temperature conundrum. Nat. Commun. 11, 4726. https://doi.org/10.1038/s41467-020-18478-6.

Berger, A., Loutre, M.-F., Yin, Q., 2010. Total irradiation during any time interval of the year using elliptic integrals. Quat. Sci. Rev. 29, 1968–1982. https://doi.org/10.1016/j.quascirev.2010.05.007.

Birks, J.B.H., Lotter, A.F., Juggins, S., Smol, J.P., 2012. Tracking Environmental Change Using Lake Sediments: Data Handling and Numerical Techniques, Developments in Paleoenvironmental Research. Springer, Netherlands.

Blaauw, M., Christen, J.A., Lopez, M.A.A., Vazquez, J.E., Belding, T., Theiler, J., Gough, B., Karney, C., 2021. rbacon: Age-Depth Modelling using Bayesian Statistics.

Bond, G., Kromer, B., Beer, J., Muscheler, R., Evans, M.N., Showers, W., Hoffmann, S., Lotti-Bond, R., Hajdas, I., Bonani, G., 2001. Persistent Solar Influence on North Atlantic climate during the Holocene. Science 294, 2130–2136. https://doi.org/10.1126/science.1065680.

Bova, S., Rosenthal, Y., Liu, Z., Godad, S.P., Yan, M., 2021. Seasonal origin of the thermal maxima at the Holocene and the last interglacial. Nature 589, 548–553. https://doi.org/10.1038/s41586-020-03155-x.

Bunn, A., Korpela, M., Biondi, F., Campelo, F., Mérian, P., Qeadan, F., Zang, C., Buras, A., Cecile, J., Mudelsee, M., Schulz, M., Stefan, K., David, F., Ronald, V., 2021. dplR: Dendrochronology Program Library in R.

Chen, F., Yu, Z., Yang, M., Ito, E., Wang, S., Madsen, D.B., Huang, X., Zhao, Y., Sato, T., John, B., Birks, H., Boomer, I., Chen, J., An, C., Wünnemann, B., 2008. Holocene moisture evolution in arid Central Asia and its out-of-phase relationship with Asian monsoon history. Quat. Sci. Rev. 27, 351–364. https://doi.org/10.1016/j.quascirev.2007.10.017.

Cheng, H., Edwards, R.L., Sinha, A., Spötl, C., Yi, L., Chen, S., Kelly, M., Kathayat, G., Wang, X., Li, X., Kong, X., Wang, Y., Ning, Y., Zhang, H., 2016. The Asian monsoon over the past 640,000 years and ice age terminations. Nature 534, 640–646. https://doi.org/10.1038/nature18591.

Cui, Q., Zhao, Y., Qin, F., Liang, C., Li, Q., Geng, R., 2019. Characteristics of the modern pollen assemblages from different vegetation zones in Northeast China: Implications for pollen-based climate reconstruction. Sci. China Earth Sci. 62, 1564–1577. https://doi.org/10.1007/s11430-018-9386-9.

Darby, D.A., Andrews, J.T., Belt, S.T., Jennings, A.E., Cabedo-Sanz, P., 2017. Holocene Cyclic Records of Ice-Rafted Debris and Sea Ice Variations on the East Greenland and Northwest Iceland Margins. Arct. Antarct. Alp. Res. 49, 649–672. https://doi.org/10.1657/AAAR0017-008.

Davis, B.A.S., Chevalier, M., Sommer, P., Carter, V.A., Finsinger, W., Mauri, A., Phelps, L. N., Zanon, M., Abegglen, R., Åkesson, C.M., Alba-Sánchez, F., Anderson, R.S., Antipina, T.G., Atanassova, J.R., Beer, R., Belyanina, N.I., Blyakharchuk, T.A., Borisova, O.K., Bozilova, E., Bukreeva, G., Bunting, M.J., Clò, E., Colombaroli, D., Combourieu-Nebout, N., Desprat, S., Di Rita, F., Djamali, M., Edwards, K.J., Fall, P. L., Feurdean, A., Fletcher, W., Florenzano, A., Furlanetto, G., Gaceur, E., Galimov, A. T., Gałka, M., García-Moreiras, I., Giesecke, T., Grindean, R., Guido, M.A., Gvozdeva, I.G., Herzschuh, U., Hjelle, K.L., Ivanov, S., Jahns, S., Jankovska, V., Jiménez-Moreno, G., Karpińska-Kołaczek, M., Kitaba, I., Kołaczek, P., Lapteva, E.G., Latałowa, M., Lebreton, V., Leroy, S., Leydet, M., Lopatina, D.A., López-Sáez, J.A., Lotter, A.F., Magri, D., Marinova, E., Matthias, I., Mavridou, A., Mercuri, A.M., Mesa-Fernández, J.M., Mikishin, Y.A., Milecka, K., Montanari, C., Morales-Molino, C., Mrotzek, A., Muñoz Sobrino, C., Naidina, O.D., Nakagawa, T., Nielsen, A.B., Novenko, E.Y., Panajiotidis, S., Panova, N.K., Papadopoulou, M., Pardoe, H.S., Pędziszewska, A., Petrenko, T.I., Ramos-Román, M.J., Ravazzi, C., Rösch, M., Ryabogina, N., Sabariego Ruiz, S., Salonen, J.S., Sapelko, T.V., Schofield, J.E., Seppä, H., Shumilovskikh, L., Stivrins, N., Stojakowits, P., Svobodova Svitavska, H., Święta-Musznicka, J., Tantau, I., Tinner, W., Tobolski, K., Tonkov, S., Tsakiridou, M., Valsecchi, V., Zanina, O.G., Zimny, M., 2020. The Eurasian Modern Pollen Database (EMPD), version 2. Earth Syst. Sci. Data 12, 2423–2445. https://doi.org/10.5194/essd-12-2423-2020.

Dong, Y., Wu, N., Li, F., Zhang, D., Zhang, Y., Shen, C., Lu, H., 2022. The Holocene temperature conundrum answered by mollusk records from East Asia. Nat. Commun. 13, 5153. https://doi.org/10.1038/s41467-022-32506-7.

Dykoski, C.A., Edwards, R.L., Cheng, H., Yuan, D., Cai, Y., Zhang, M., Lin, Y., Qing, J., An, Z., Revenaugh, J., 2005. A high-resolution, absolute-dated Holocene and deglacial Asian monsoon record from Dongge Cave. China. Earth Planet. Sci. Lett. 233, 71–86. https://doi.org/10.1016/j.epsl.2005.01.036.

Faegri, K., Iversen, J., Kaland, P.E., Krzywinski, K., 2000. Textbook of Pollen Analysis, 4th ed. The Blackburn Press, Caldwell, NJ.

Gao, G., Jie, D., Li, D., Li, N., Liu, L., Liu, H., Shi, J., Leng, C., Wang, J., Liu, B., Li, P., 2018. Reliability of phytoliths for reconstructing vegetation dynamics in northern temperate forest regions: a case study in Northeast China. Quat. Sci. Rev. 201, 1–12. https://doi.org/10.1016/j.quascirev.2018.10.020.

Geng, R., Zhao, Y., Cui, Q., Qin, F., 2019. Representation of modern pollen assemblages with respect to vegetation and climate in Northeast China. Quat. Int. 532, 126–137. https://doi.org/10.1016/j.quaint.2019.11.003.

Geng, R., Andreev, A., Kruse, S., Heim, B., van Geffen, F., Pestryakova, L., Zakharov, E., Troeva, E., Shevtsova, I., Li, F., Zhao, Y., Herzschuh, U., 2022. Modern pollen assemblages from lake sediments and soil in east siberia and relative pollen productivity estimates for major taxa. Front. Ecol. Evol. 10.

Greenwell, B., Boehmke, B., Cunningham, J., 2022. Developers (https://github.com/gbm-developers), G.B.M., 2022. gbm: Generalized Boosted Regression Models.

Hammer, Ø., Harper, D.A.T., Ryan, P.D., 2001. Past: paleontological statistics software package for education and data analysis. Palaeontol. Electron. 4.

He, S., Gao, Y., Li, F., Wang, H., He, Y., 2017. Impact of Arctic Oscillation on the East Asian climate: a review. Earth Sci. Rev. 164, 48–62. https://doi.org/10.1016/j.earscirev.2016.10.014.

Herzschuh, U., Borkowski, J., Schewe, J., Mischke, S., Tian, F., 2014. Moisture-advection feedback supports strong early-to-mid Holocene monsoon climate on the eastern Tibetan Plateau as inferred from a pollen-based reconstruction. Palaeogeogr. Palaeoclimatol. Palaeoecol. 402, 44–54. https://doi.org/10.1016/j.palaeo.2014.02.022.

Herzschuh, U., Cao, X., Laepple, T., Dallmeyer, A., Telford, R.J., Ni, J., Chen, F., Kong, Z., Liu, G., Liu, K.-B., Liu, X., Stebich, M., Tang, L., Tian, F., Wang, Y., Wischnewski, J., Xu, Q., Yan, S., Yang, Z., Yu, G., Zhang, Y., Zhao, Y., Zheng, Z., 2019. Position and orientation of the westerly jet determined Holocene rainfall patterns in China. Nat. Commun. 10, 2376. https://doi.org/10.1038/s41467-019-09866-8.

Hou, X., 2001. 1:1000000 Vegetation Altas of China. Science Press, Beijing.

Jiang, D., Lang, X., Tian, Z., Wang, T., 2012. Considerable model–data mismatch in temperature over china during the mid-holocene: results of PMIP simulations. J. Climate 25, 4135–4153. https://doi.org/10.1175/JCLI-D-11-00231.1.

Juggins, S., 2022. rioja: Analysis of Quaternary Science Data.

Kaboth-Bahr, S., Bahr, A., Zeeden, C., Yamoah, K.A., Lone, M.A., Chuang, C.-K., Löwemark, L., Wei, K.-Y., 2021. A tale of shifting relations: East Asian summer and winter monsoon variability during the Holocene. Sci. Rep. 11, 6938. https://doi.org/10.1038/s41598-021-85444-7.

Kang, S., Wang, X., Roberts, H.M., Duller, G.A.T., Cheng, P., Lu, Y., An, Z., 2018. Late Holocene anti-phase change in the East Asian summer and winter monsoons. Quat. Sci. Rev. 188, 28–36. https://doi.org/10.1016/j.quascirev.2018.03.028.

Kaufman, D.S., Broadman, E., 2023. Revisiting the Holocene global temperature conundrum. Nature 614, 425–435. https://doi.org/10.1038/s41586-022-05536-w.

Kaufman, D., McKay, N., Routson, C., Erb, M., Dätwyler, C., Sommer, P.S., Heiri, O., Davis, B., 2020. Holocene global mean surface temperature, a multi-method reconstruction approach. Sci. Data 7, 201. https://doi.org/10.1038/s41597-020-0530-7.

Leng, C., 2019. Phytolith Record of High Resolution Climate Change in Gushantun Peatland since Last Glacial Age (Master). Northeast Normal University.

Li, C., Wu, Y., Hou, X., 2011. Holocene vegetation and climate in Northeast China revealed from Jingbo Lake sediment. Quat. Int. 229, 67–73. https://doi.org/10.1016/j.quaint.2009.12.015.

Li, N., Chambers, F.M., Yang, J., Jie, D., Liu, L., Liu, H., Gao, G., Gao, Z., Li, D., Shi, J., Feng, Y., Qiao, Z., 2017. Records of East Asian monsoon activities in Northeastern China since 15.6 ka, based on grain size analysis of peaty sediments in the Changbai Mountains. Quat. Int. 447, 158–169. https://doi.org/10.1016/j.quaint.2017.03.064.

Li, N., Li, M., Sack, D., Kang, W., Song, L., Yang, Y., Zong, Y., Jie, D., 2020. Diatom evidence for mid-Holocene peatland water-table variations and their possible link to solar forcing. Sci. Total Environ. 725, 138272 https://doi.org/10.1016/j.scitotenv.2020.138272.

Liang, C., Zhao, Y., Qin, F., Zheng, Z., Xiao, X., Ma, C., Li, H., Zhao, W., 2020. Pollen-based Holocene quantitative temperature reconstruction on the eastern Tibetan Plateau using a comprehensive method framework. Sci. China Earth Sci. 63, 1144–1160. https://doi.org/10.1007/s11430-019-9599-y.

Liu, J., 1989. Vegetational and climatic changes at Gushantun Bog in Jilin, NE China since 13000 Y. BP. Acta Palaeontol. Sin. 28, 495–511.

Liu, Z., Otto-Bliesner, B.L., He, F., Brady, E.C., Tomas, R., Clark, P.U., Carlson, A.E., Lynch-Stieglitz, J., Curry, W., Brook, E., Erickson, D., Jacob, R., Kutzbach, J., Cheng, J., 2009. Transient simulation of last Deglaciation with a New Mechanism for Bølling-Allerød Warming. Science 325, 310–314. https://doi.org/10.1126/science.1171041.

Liu, Z., Zhu, J., Rosenthal, Y., Zhang, X., Otto-Bliesner, B.L., Timmermann, A., Smith, R. S., Lohmann, G., Zheng, W., Timm, O.E., 2014. The Holocene temperature conundrum. Proc. Natl. Acad. Sci. 111, E3501–E3505. https://doi.org/10.1073/pnas.1407229111.

Liu, Y., Zhang, M., Liu, Z., Xia, Y., Huang, Y., Peng, Y., Zhu, J., 2018. A possible Role of Dust in Resolving the Holocene Temperature Conundrum. Sci. Rep. 8, 4434. https://doi.org/10.1038/s41598-018-22841-5.

Liu, X., Zhan, T., Zhou, Xinying, Wu, H., Li, Q., Zhao, C., Qiao, Y., Jiang, S., Tu, L., Ma, Y., Zhang, J., Jiang, X., Lou, B., Zhang, X., Zhou, Xin, 2019. Late onset of the Holocene rainfall maximum in northeastern China inferred from a pollen record from the sediments of Tianchi Crater Lake. Quatern. Res. 92, 133–145. https://doi.org/10.1017/qua.2018.137.

Ma, Q., Zhu, L., Lu, X., Wang, Y., Guo, Y., Wang, J., Ju, J., Peng, P., Tang, L., 2017. Modern pollen assemblages from surface lake sediments and their environmental implications on the southwestern Tibetan Plateau. Boreas 46, 242–253. https://doi.org/10.1111/bor.12201.

Ma, L., Gao, C., Kattel, G.R., Yu, X., Wang, G., 2018. Evidence of Holocene water level changes inferred from diatoms and the evolution of the Honghe Peatland on the Sanjiang Plain of Northeast China. Quat. Int. 476, 82–94. https://doi.org/10.1016/j.quaint.2018.02.025.

Mann, M.E., Schmidt, G.A., Miller, S.K., LeGrande, A.N., 2009a. Potential biases in inferring Holocene temperature trends from long-term borehole information. Geophys. Res. Lett. 36 https://doi.org/10.1029/2008GL036354.

Mann, M.E., Schmidt, G.A., Miller, S.K., LeGrande, A.N., 2009b. Potential biases in inferring Holocene temperature trends from long-term borehole information. Geophys. Res. Lett. 36 https://doi.org/10.1029/2008GL036354.

Marcott, S.A., Shakun, J.D., Clark, P.U., Mix, A.C., 2013. A Reconstruction of Regional and Global Temperature for the past 11,300 years. Science 339, 1198–1201. https://doi.org/10.1126/science.1228026.

Marsicek, J., Shuman, B.N., Bartlein, P.J., Shafer, S.L., Brewer, S., 2018. Reconciling divergent trends and millennial variations in Holocene temperatures. Nature 554, 92–96. https://doi.org/10.1038/nature25464.

Meyers, S., Malinverno, A., Hinnov, L., Zeeden, C., Liu, H., Moron, V., 2021. astrochron: A Computational Tool for Astrochronology.

Oksanen, J., Blanchet, F.G., Friendly, M., Kindt, R., Legendre, P., McGlinn, D., Minchin, P.R., O'Hara, R.B., Simpson, G.L., Solymos, P., Stevens, M.H.H., Szoecs, E., Wagner, H., 2019. vegan: Community Ecology Package.

Pei, Q., Zhang, D.D., Li, J., Fei, J., 2019. Proxy-based temperature reconstruction in China for the Holocene. Quat. Int. 521, 168–174. https://doi.org/10.1016/j.quaint.2019.06.032.

R Core Team, 2019. R: A Language and Environment for Statistical Computing. R Foundation for Statistical Computing, Vienna, Austria.

Ran, M., Feng, Z., 2013. Holocene moisture variations across China and driving mechanisms: a synthesis of climatic records. In: Quat. Int., Proxies for Quaternary monsoon reconstruction on the Tibetan Plateau, 313–314, pp. 179–193. https://doi.org/10.1016/j.quaint.2013.09.034.

Reimer, P.J., Bard, E., Bayliss, A., Beck, J.W., Blackwell, P.G., Ramsey, C.B., Buck, C.E., Cheng, H., Edwards, R.L., Friedrich, M., Grootes, P.M., Guilderson, T.P., Haflidason, H., Hajdas, I., Hatté, C., Heaton, T.J., Hoffmann, D.L., Hogg, A.G., Hughen, K.A., Kaiser, K.F., Kromer, B., Manning, S.W., Niu, M., Reimer, R.W., Richards, D.A., Scott, E.M., Southon, J.R., Staff, R.A., Turney, C.S.M., Plicht, J., 2013. IntCal13 and Marine13 Radiocarbon Age Calibration Curves 0–50,000 years cal BP. Radiocarbon 55, 1869–1887. https://doi.org/10.2458/azu_js_rc.55.16947.

Schulz, M., Mudelsee, M., 2002. REDFIT: estimating red-noise spectra directly from unevenly spaced paleoclimatic time series. Comput. Geosci. 28, 421–426. https://doi.org/10.1016/S0098-3004(01)00044-9.

Simpson, G.L., Oksanen, J., Maechler, M., 2021. analogue: Analogue and Weighted Averaging Methods for Palaeoecology.

Solanki, S.K., Usoskin, I.G., Kromer, B., Schüssler, M., Beer, J., 2004. Unusual activity of the Sun during recent decades compared to the previous 11,000 years. Nature 431, 1084–1087. https://doi.org/10.1038/nature02995.

Stebich, M., Rehfeld, K., Schlütz, F., Tarasov, P.E., Liu, J., Mingram, J., 2015. Holocene vegetation and climate dynamics of NE China based on the pollen record from Sihailongwan Maar Lake. Quat. Sci. Rev. 124, 275–289. https://doi.org/10.1016/j.quascirev.2015.07.021.

Stockmarr, J., 1971. Tablets with spores used in absolute pollen analysis. Pollen Spores 13, 615–621.

Sun, J., Ma, C., Cao, X., Zhao, Y., Deng, Y., Zhao, L., Zhu, C., 2019. Quantitative precipitation reconstruction in the east-central monsoonal China since the late glacial period. Quat. Int. 521, 175–184. https://doi.org/10.1016/j.quaint.2019.05.033.

Tang, L., Mao, L., Shu, J., Li, C., Shen, C., Zhou, Z., 2016. An Illustrated Handbook of Quaternary Pollen and Spores in China (in Chinese with English Summary), 1st ed. Science Press Ltd, Beijing.

Tarasov, P.E., Nakagawa, T., Demske, D., Österle, H., Igarashi, Y., Kitagawa, J., Mokhova, L., Bazarova, V., Okuda, M., Gotanda, K., Miyoshi, N., Fujiki, T., Takemura, K., Yonenobu, H., Fleck, A., 2011. Progress in the reconstruction of Quaternary climate dynamics in the Northwest Pacific: a new modern analogue reference dataset and its application to the 430-kyr pollen record from Lake Biwa. Earth Sci. Rev. 108, 64–79. https://doi.org/10.1016/j.earscirev.2011.06.002.

Telford, R.J., Birks, H.J.B., 2011. A novel method for assessing the statistical significance of quantitative reconstructions inferred from biotic assemblages. Quat. Sci. Rev. 30, 1272–1278. https://doi.org/10.1016/j.quascirev.2011.03.002.

Telford, R., Trachsel, M., 2019. palaeoSig: Significance Tests for Palaeoenvironmental Reconstructions.

Thompson, A.J., Zhu, J., Poulsen, C.J., Tierney, J.E., Skinner, C.B., 2022. Northern Hemisphere vegetation change drives a Holocene thermal maximum. Sci. Adv. 8, eabj6535. https://doi.org/10.1126/sciadv.abj6535.

Torrence, C., Compo, G.P., 1998. A Practical Guide to Wavelet Analysis. Bull. Am. Meteorol. Soc. 79, 61–78. https://doi.org/10.1175/1520-0477(1998)079<0061:APGTWA>2.0.CO;2.

Turney, C., Baillie, M., Clemens, S., Brown, D., Palmer, J., Pilcher, J., Reimer, P., Leuschner, H.H., 2005. Testing solar forcing of pervasive Holocene climate cycles. J. Quat. Sci. 20, 511–518. https://doi.org/10.1002/jqs.927.

Wang, F., 1995. Pollen Flora of China. Science Press, Beijing.

Wang, Y., Cheng, H., Edwards, R.L., Kong, X., Shao, X., Chen, S., Wu, J., Jiang, X., Wang, X., An, Z., 2008. Millennial- and orbital-scale changes in the East Asian monsoon over the past 224,000 years. Nature 451, 1090–1093. https://doi.org/10.1038/nature06692.

Wang, W., Liu, L., Li, Y., Niu, Z., He, J., Ma, Y., Mensing, S.A., 2019. Pollen reconstruction and vegetation dynamics of the middle Holocene maximum summer monsoon in northern China. Palaeoclimatol. Palaeoecol. 528, 204–217. https://doi.org/10.1016/j.palaeo.2019.05.023.

Wassenburg, J.A., Dietrich, S., Fietzke, J., Fohlmeister, J., Jochum, K.P., Scholz, D., Richter, D.K., Sabaoui, A., Spötl, C., Lohmann, G., Andreae, M.O., Immenhauser, A., 2016. Reorganization of the North Atlantic Oscillation during early Holocene deglaciation. Nat. Geosci. 9, 602–605. https://doi.org/10.1038/ngeo2767.

Wen, R., Xiao, J., Ma, Y., Feng, Z., Li, Y., Xu, Q., 2013. Pollen–climate transfer functions intended for temperate eastern Asia. In: Quat. Int., Hydrological and Ecological Responses to Climatic Change and to Land-use/land-cover changes in Central Asia, 311, pp. 3–11. https://doi.org/10.1016/j.quaint.2013.04.025.

Wu, J., Liu, Q., Wang, X., Chu, G., Liu, J., 2016. Vegetation and climate change during the last deglaciation in the Great Khingan Mountain, Northeastern China. PLOS ONE 11, e0146261. https://doi.org/10.1371/journal.pone.0146261.

Wu, J., Shen, C., Yang, H., Qian, S., Xie, S., 2023. Holocene temperature variability in China. Quat. Sci. Rev. 312, 108184 https://doi.org/10.1016/j.quascirev.2023.108184.

Xu, Q., Xiao, J., Li, Y., Tian, F., Nakagawa, T., 2010. Pollen-based Quantitative Reconstruction of Holocene climate changes in the Daihai Lake Area, Inner

Mongolia, China. J. Clim. 23, 2856–2868. https://doi.org/10.1175/2009JCLI3155.1.

Xu, D., Lu, H., Chu, G., Liu, L., Shen, C., Li, F., Wang, C., Wu, N., 2019. Synchronous 500-year oscillations of monsoon climate and human activity in Northeast Asia. Nat. Commun. 10, 4105. https://doi.org/10.1038/s41467-019-12138-0.

Yoshida, A., Takeuti, S., 2009. Quantitative reconstruction of palaeoclimate from pollen profiles in northeastern Japan and the timing of a cold reversal event during the last termination. J. Quat. Sci. 24, 1006–1015. https://doi.org/10.1002/jqs.1284.

Zhang, Z., Leduc, G., Sachs, J.P., 2014. El Niño evolution during the Holocene revealed by a biomarker rain gauge in the Galápagos Islands. Earth Planet. Sci. Lett. 404, 420–434. https://doi.org/10.1016/j.epsl.2014.07.013.

Zhang, Y., Renssen, H., Seppä, H., Valdes, P.J., 2017. Holocene temperature evolution in the Northern Hemisphere high latitudes – Model-data comparisons. Quat. Sci. Rev. 173, 101–113. https://doi.org/10.1016/j.quascirev.2017.07.018.

Zhang, Y., Renssen, H., Seppä, H., Valdes, P.J., 2018. Holocene temperature trends in the extratropical Northern Hemisphere based on inter-model comparisons. J. Quat. Sci. 33, 464–476. https://doi.org/10.1002/jqs.3027.

Zhang, H., Ait Brahim, Y., Li, H., Zhao, J., Kathayat, G., Tian, Y., Baker, J., Wang, J., Zhang, F., Ning, Y., Edwards, R.L., Cheng, H., 2019. The Asian Summer Monsoon: Teleconnections and Forcing Mechanisms—a Review from Chinese Speleothem δ18O Records. Quaternary 2, 26. https://doi.org/10.3390/quat2030026.

Zhang, W., Wu, H., Cheng, J., Geng, J., Li, Q., Sun, Y., Yu, Y., Lu, H., Guo, Z., 2022. Holocene seasonal temperature evolution and spatial variability over the Northern Hemisphere landmass. Nat. Commun. 13, 5334. https://doi.org/10.1038/s41467-022-33107-0.

Zhao, Y., 2018. Vegetation and climate reconstructions on different time scales in China: a review of Chinese palynological research. Veg. Hist. Archaeobotany 27, 381–392. https://doi.org/10.1007/s00334-017-0655-6.

Zhao, Y., Yu, Z., 2012. Vegetation response to Holocene climate change in East Asian monsoon-margin region. Earth Sci. Rev. 113, 1–10. https://doi.org/10.1016/j.earscirev.2012.03.001.

Zhao, Y., Liang, C., Cui, Q., Qin, F., Zheng, Z., Xiao, X., Ma, C., Felde, V.A., Liu, Y., Li, Q., Zhang, Z., Herzschuh, U., Xu, Q., Wei, H., Cai, M., Cao, X., Guo, Z., Birks, H.J.B.,

2021. Temperature reconstructions for the last 1.74-Ma on the eastern Tibetan Plateau based on a novel pollen-based quantitative method. Glob. Planet. Change 199, 103433. https://doi.org/10.1016/j.gloplacha.2021.103433.

Zheng, Z., Wei, J., Huang, K., Xu, Q., Lu, H., Tarasov, P., Luo, C., Beaudouin, C., Deng, Y., Pan, A., Zheng, Y., Luo, Y., Nakagawa, T., Li, C., Yang, S., Peng, H., Cheddadi, R., 2014. East Asian pollen database: modern pollen distribution and its quantitative relationship with vegetation and climate. J. Biogeogr. 41, 1819–1832. https://doi.org/10.1111/jbi.12361.

Zheng, Z., Zhang, X., Man, M., Wei, J., Huang, K., 2016. Review and data integration of pollen-based quantitative paleoclimate reconstruction studies in China and adjacent areas (in Chinese). Quat. Sci. 36, 503–519. https://doi.org/10.11928/j.issn.1001-7410.2016.03.01.

Zheng, Y., Pancost, R.D., Liu, X., Wang, Z., Naafs, B.D.A., Xie, X., Liu, Z., Yu, X., Yang, H., 2017. Atmospheric connections with the North Atlantic enhanced the deglacial warming in Northeast China. Geology 45, 1031–1034. https://doi.org/10.1130/G39401.1.

Zheng, Y., Pancost, R.D., Naafs, B.D.A., Li, Q., Liu, Z., Yang, H., 2018. Transition from a warm and dry to a cold and wet climate in NE China across the Holocene. Earth Planet. Sci. Lett. 493, 36–46. https://doi.org/10.1016/j.epsl.2018.04.019.

Zhou, Y., 1997. Geography of the Vegetation in Northeast China. Science Press, Beijing.

Zhou, W., Zheng, Y., Meyers, P.A., Jull, A.J.T., Xie, S., 2010. Postglacial climate-change record in biomarker lipid compositions of the Hani peat sequence, Northeastern China. Earth Planet. Sci. Lett. 294, 37–46. https://doi.org/10.1016/j.epsl.2010.02.035.

Zhou, Xin, Sun, L., Zhan, T., Huang, W., Zhou, Xinying, Hao, Q., Wang, Y., He, X., Zhao, C., Zhang, J., Qiao, Y., Ge, J., Yan, P., Yan, Q., Shao, D., Chu, Z., Yang, W., Smol, J.P., 2016. Time-transgressive onset of the Holocene Optimum in the East Asian monsoon region. Earth Planet. Sci. Lett. 456, 39–46. https://doi.org/10.1016/j.epsl.2016.09.052.

Zuo, J., Ren, H.-L., Li, W., 2015. Contrasting impacts of the arctic oscillation on surface air temperature anomalies in Southern China between early and middle-to-late winter. J. Climate 28, 4015–4026. https://doi.org/10.1175/JCLI-D-14-00687.1.